How To Make Nitroaromatic Compounds Glow: Next-Generation Large X-Shaped, Centrosymmetric Diketopyrrolopyrroles

Kamil Skonieczny, Ilias Papadopoulos, Dominik Thiel, Krzysztof Gutkowski, Philipp Haines, Patrick Mccosker, Adele D. Laurent, Paul Keller, Timothy Clark, Denis Jacquemin, et al.

RESEARCH ARTICLE

How to Make Nitroaromatics Glow: Next Generation Large, χ—Shaped, Centrosymmetric Diketopyrrolopyrroles

Kamil Skonieczny,‡ [a] Ilias Papadopoulos,‡ [b] Dominik Thiel,‡ [b] Krzysztof Gutkowski,[a] Philipp Haines,[b] Patrick M. McCosker,[c,d,e] Adèle D. Laurent,[f] Paul A. Keller,[d,e] Timothy Clark,[c] Denis Jacquemin,*[f] Dirk M. Guldi*[b] and Daniel T. Gryko*[a]

Dedicated to Prof. Lechosław Latos-Grażyński on his 70th birthday

Abstract: This article describes a synthetic approach to a new structurally diverse family of π-expanded diketopyrrolopyrroles (DPPs). These red-emissive dyes, based on a previously unknown skeleton, can be easily synthesized *via* a three-step strategy involving the preparation of diketopyrrolopyrrole followed by *N*-arylation and subsequent intramolecular palladium-catalyzed direct arylation. A careful selection of the aryl substituents on DPP gives access to a π-extended DPP derivative with intense fluorescence reaching 750 nm. The fact that NO_2 groups do not engage in the excited states is responsible for the lack of fluorescence quenching when this functional group is present. Comprehensive spectroscopic assays combined with first principle calculations corroborated that both *N*-arylated and fused DPPs reach a locally excited (S_1) state after excitation, followed by internal conversion to states with solvent and structural relaxation, before eventually undergoing intersystem crossing. Only the structurally relaxed state is fluorescent with lifetimes in the range of several nanoseconds and tens of picoseconds in non-polar and polar solvents, respectively. The aforementioned lifetimes correlate with fluorescence quantum yields, which range from 6% to 88% in non-polar solvents and from 0.4% and 3.2% in polar solvents. For the fully fused DPP a very inefficient (T_1) population is responsible for fluorescence quantum yields as high as 88% in polar solvents, which is among the uppermost ever recorded for nitro-aromatics. These findings demonstrate the immense importance of the ability to design, build and fine-tune the structure of large, π-expanded functional dyes so that the strong polarization of centrosymmetric structures is achieved.

Introduction

A significant number of heterocyclic analogs of nanographenes are known to date,[1,2] yet the overwhelming majority lack electron-withdrawing and/or electron-donating groups and, hence, remain unpolarized. This can be attributed to significant difficulties originating from the lack of compatibility between required functional groups and the synthetic methodologies used. To achieve such goal, rather than decorating large π-systems with electron-withdrawing and electron-donating substituents, one may envision the use of highly polarized heterocyclic scaffolds. Along these lines, a family of cross-conjugated, donor-acceptor chromophores are plausibly the best candidates. Among the cross-conjugated chromophores,[3] such as indigos,[4] isoindigos,[5] bay-annulated indigos,[6] quinacridones,[4a] epindolindiones[4b,6] and dipyrrolonaphthyridinediones,[7] diketopyrrolopyrroles (DPPs)[8,9,10] are unique by virtue of two major reasons: (1) they are the most intensively probed material in the field of organic electronics and photonics in recent decades;[11,12] and (2) their synthetic chemistry is the most developed, opening in principle unlimited possibilities for tailored modifications.[13]

The functional groups present in the core structure of DPPs serve as a starting point towards the design of novel architectures possessing π-expanded chromophores.[14] Only four different strategies aiming at the π-expansion of DPPs have been presented so far.[15-18] In each case, novel materials with intriguing photophysical features have been obtained (Fig. 1).[19] It is clear that new combinations and fusions of DPPs with other scaffolds may provide access to unprecedented functional dyes, which may retain some advantageous properties of DPP, yet extend beyond their typical photophysics. Along these lines, we envisioned another strategy enabling unlimited structural modifications and leading, in turn, to unprecedented photophysical properties. In parallel, in light of the nitro functional groups role as a notorious, although quite mysterious, quencher of fluorescence,[20] we are interested in shedding light onto the influence nitro groups have on DPPs emission. Last but not least, we were eager to probe the effect of symmetry. This latter interest relates to the specific framework of symmetry breaking in quadrupolar centrosymmetric dyes.[21]

[a] Dr. Kamil Skonieczny, Krzysztof Gutkowski, Prof. Daniel T. Gryko, Institute of Organic Chemistry PAS. 44/52 Kasprzaka, 01-224 Warsaw, Poland. E-mail: dtgryko@icho.edu.pl

[b] Ilias Papadopoulos, Dominik Thiel, Philipp Haines, Prof. Dirk M. Guldi, Department of Chemistry and Pharmacy & Interdisciplinary Center for Molecular Materials (ICMM), Friedrich-Alexander-Universität Erlangen-Nürnberg (FAU), Egerlandstr. 3, 91058 Erlangen, Germany. E-mail: dirk.guldi@fau.de

[c] Patrick M. McCosker, Prof. Timothy Clark, Department of Chemistry and Pharmacy & Computer-Chemie-Center (CCC), Friedrich-Alexander-Universität Erlangen-Nürnberg, Nägelsbachstr. 25, 91052 Erlangen, Germany. E-mail: tim.clark@fau.de

[d] Patrick M. McCosker, Prof. Paul A. Keller, School of Chemistry & Molecular Bioscience, Molecular Horizons, University of Wollongong, NSW 2522, Australia. E-mail: keller@uow.edu.au

[e] Patrick M. McCosker, Prof. Paul A. Keller, Illawarra Health & Medical Research Institute, Wollongong, NSW 2522, Australia. E-mail: keller@uow.edu.au

[f] Adèle D. Laurent, Prof. Denis Jacquemin, Université de Nantes, CNRS, CEISAM UMR 6230, Nantes, France. Denis.Jacquemin@univ-nantes.fr

‡ These authors contributed equally.

Electronic Supplementary Information (ESI) available: [synthetic procedures, analytical data, advanced photophysical data and details of computational studies]. See DOI: 10.1039/x0xx00000x

Supporting information for this article is given via a link at the end of the document.

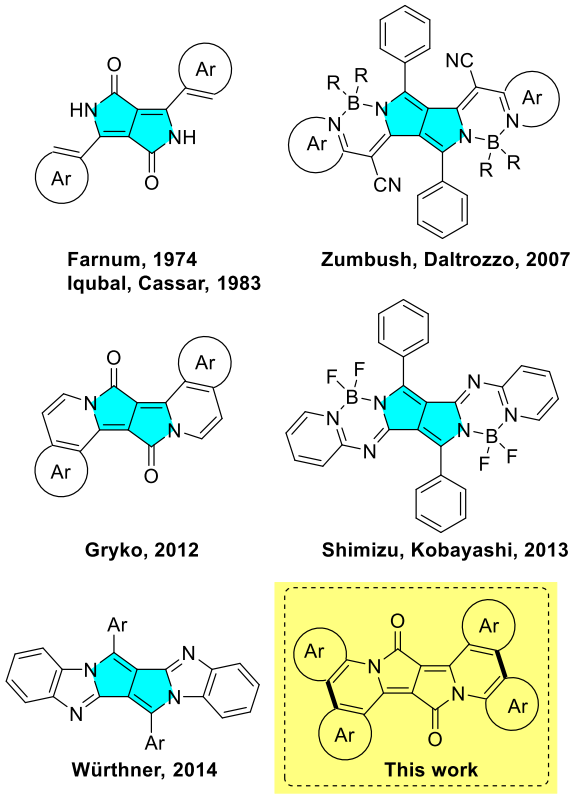

Figure 1. The history of π-expanded diketopyrrolopyrroles.

Herein, we provide the first examples of χ-shaped, highly polarized, π-expanded diketopyrrolopyrroles, using *N*-arylation of DPPs followed by an intramolecular direct arylation of the aromatic rings that are present in these building blocks.

Results and Discussion

Design and synthesis

The construction of π-expanded DPPs requires installation of two aryl substituents, possessing bromine atoms adjacent to the linking positions on the DPP nitrogen atoms. This calls for 1-fluoro-2-bromobenzenes. One of the key problems in the chemistry of DPPs is, however, the limited scope of *N*-arylation. The ubiquitous presence of the bis-*N*-alkylated DPPs[8,10,22] contrasts with the scarcity of bis-*N*-arylated DPPs.[23-25]

The most intuitive approach is based on the reaction between a corresponding aryl fluoride and DPP in the presence of a base. Thus, to accomplish our goal, we began by testing the activity of commercially available 3-bromo-4-fluoronitrobenzene in DPP arylation. In this case, however, we only obtained a mono-arylation product with a low yield (15%). In the light of this result, we resolved to the 2-fluoropyridine derivative which would be more reactive S_NAr. 3-Bromo-2-fluoro-5-nitropyridine was generated *in situ* by three hours heating of 3-bromo-2-chloro-5-nitropyridine (**1**) in DMF in the presence of KF.[26]

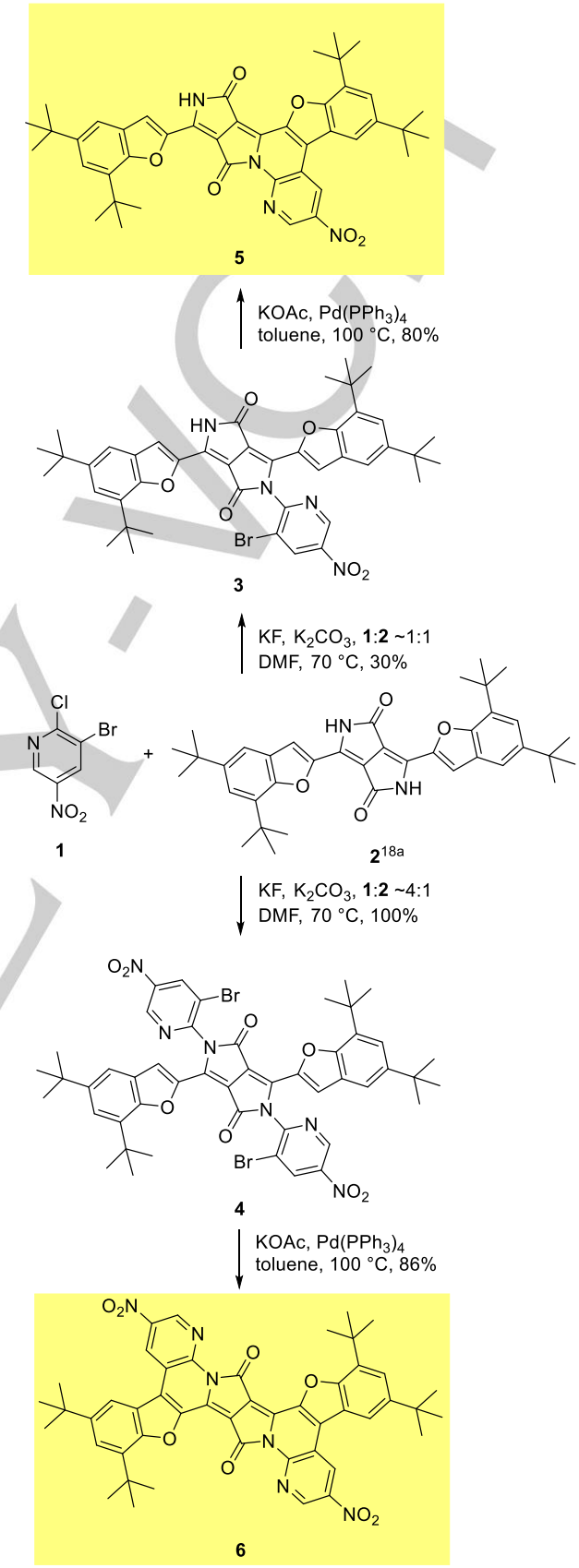

Scheme 1. The synthesis of π-expanded diketopyrrolopyrroles **5** and **6**.

It turned out that DPP **2** easily reacted with 3-bromo-2-fluoro-5-nitropyridine in the presence of potassium carbonate in DMF at 70 °C to give the corresponding *N*-arylated DPPs, which enabled the implementation of a "one pot" procedure (Scheme 1). Reaction with 1.2 equivalents (or less) of the aryl fluoride, produced a mixture of products which, in addition to the expected mono-arylated DPP **3**, also contained unreacted substrate and a significant amount of diarylated DPP **4**. By increasing the amount of aryl fluoride to reach 4 equivalents we obtained bis-*N*,*N*-arylated DPP **4** in a pure form by crystallization from the reaction mixture. The bis-arylation reaction was essentially quantitative in this case. In the next step, both **3** and **4** were subjected to the KOAc and $Pd(PPh_3)_4$ conditions developed by various groups for intramolecular direct arylation of aromatic and heteroaromatic systems.[27] We achieved both π-expanded products **5** and **6** with good yields when the reaction was carried out 24 h in dry toluene at 100 °C.

Photophysical properties

Steady-State Absorption Spectroscopy

Absorption experiments with dyes **3**–**6** in toluene reveal S_0-S_1 absorption maxima in the 450 to 660 nm range (Table 1, Figure 2). Depending on the size of the π-conjugated system, the absorption maxima are shifted to longer wavelengths in the following order: **3** < **4** < **5** < **6**. DPP **3**, for example, features the smallest π-conjugated system and, consequently, gives rise to absorption maxima at 453, 489, 522 and 567 nm due to vibronic couplings (*vide infra*).

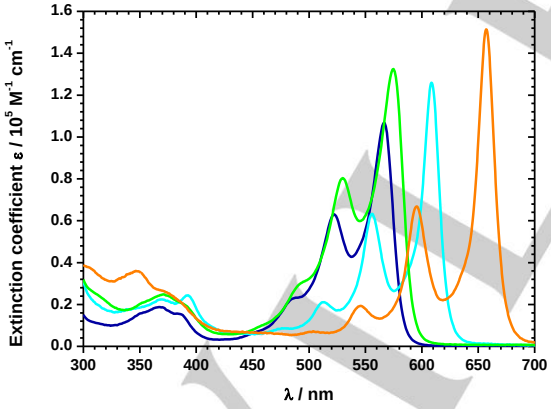

Figure 2. Room temperature absorption spectra of **3** (dark blue), **4** (green), **5** (pale blue) and **6** (orange) in toluene.

Di-*N*-arylated DPP **4** has the lowest energy absorption maximum at 578 nm in toluene which corresponds nicely with two previously studied di-*N*-arylated DPPs possessing 5,7-bis(*tert*-butyl)benzofuranyl substituents (578 and 588 nm in DCM).[24,25] In stark contrast, DPP **6**, which has the most extended π-conjugated skeleton, shows a vibronic progression with maxima at 504, 545, 595, and 657 nm. Upon increasing the solvent polarity stepwise, that is, going from toluene *via* anisole and chlorobenzene to benzonitrile, a limited solvatochromatic red-shift is noted for dyes **3**–**6**. This is accompanied by a steady decrease in extinction coefficients (Supplementary Figure S1-S4).

Steady-State Fluorescence Spectroscopy

Next, we set our focus on the excited states (ES) by means of steady-state fluorescence spectroscopy. In toluene, the fluorescence spectra of **3**–**6** are mirror-images of the absorption spectra with maxima in the range of 575 to 735 nm, and similar vibronic progressions. The Stokes shifts are less than 10 nm (Figures 2 and 3). In a similar manner to the absorption features, the fluorescence maxima of **3**–**6** exhibit a dependence on the size of the π-conjugated system and shift to longer wavelengths as a function of size (Tables 1-2). The fluorescence quantum yields (Φ_{fl}) also increase in the following order: **3** < **4** < **5** < **6**, that is, the higher the rigidity of the fused system, the larger Φ_{fl}. Φ_{fl} is markedly larger for π-expanded DPPs **5** and **6** reaching around 39% and 88% in non-polar solvents (Table 1), respectively. As a matter of fact, fluorescence quantum yields are comparable to those measured for previously reported π-expanded DPPs bearing two benzofuran units, but lacking two arene rings and nitro groups.[18a] Our observations suggest that no significant quenching stems from the nitro groups.

Table 1. Fundamental photophysical properties of DPPs **3**-**6** in toluene.

Compound	λ_{abs} (nm)	ε ($10^4 M^{-1}cm^{-1}$)	λ_{em} (nm)	Φ_{fl} (%)
3	567, 522	10.8	575, 625	6
4	575, 530	13.0	585, 636	35
5	609, 556	12.6	615, 676	39
6	657, 595	14.6	663, 735	88

The absorption and fluorescence maxima of dyes **3-6** were scarcely affected by the dielectric constants of the solvents, whereas the Φ_{fl} varied significantly (Table 2, Figures S5-S8). DPPs **3**–**5** exhibit by far the highest values in toluene. Only a slight increase of the polarity, by, for example, going from toluene to anisole, leads to a strong decrease of Φ_{fl}. A further increase in polarity to chlorobenzene and to benzonitrile leads to even lower quantum yields with values of less than 1%. Important is the fact that the spectral shape of the fluorescence remains largely unchanged in the different solvents excluding discernable charge-transfer contributions in the fluorescent decay.

Table 2: Fluorescence quantum yields (%) of dyes **3**-**6** in toluene, anisole, chlorobenzene, and benzonitrile. The fluorescence references used for determining the quantum yields are Rhodamine B for **3** and **4**, Sulforhodamine 101 for **5** and Nile Blue for **6**.

	Toluene	Anisole	Chlorobenzene	Benzonitrile
3	6	0.6	0.5	0.4
4	35	0.5	0.3	0.2
5	39	1.8	2.9	0.6

6	88	58	59	3.2

DPP **6** is a notable exception as a change from toluene to anisole or chlorobenzene reduces the fluorescence quantum yield from 88% to only 58%. It is only in benzonitrile that the drop is significant and quantum yields as low as 3.2% are observed (Supplementary Figures S5-S8). The fact that planarization of the chromophore bearing nitroaryl groups makes the emission intensity of the π-system less susceptible to increasing solvent polarity has been already observed by us while studying dinitro-pyrrolo[3,2-*b*]pyrroles.[28]

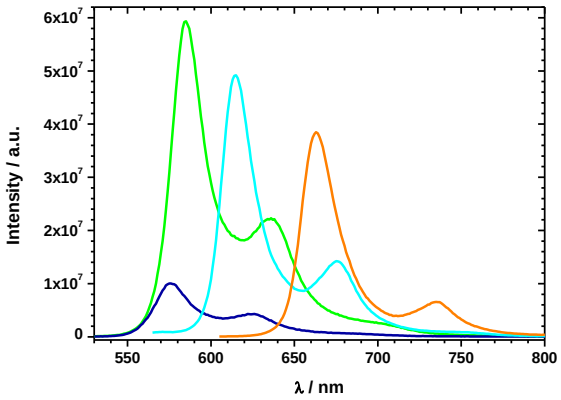

Figure 3. Room temperature fluorescence spectra of **3** (dark blue), **4** (green), **5** (pale blue) and **6** (orange) (3×10^{-6} M) in toluene with excitation wavelengths of 515, 515, 550 and 590 nm, respectively.

Time Correlated Single Photon Counting (TCSPC)

Time-resolved fluorescence measurements with dyes **3**–**6** were carried out in toluene as well as in benzonitrile. In toluene, all lifetimes are best described by monoexponential decay rates with values around 4 ns. Significant differences were seen in benzonitrile. Here, the fluorescence lifetimes are less than 200 ps (Table 3). Our findings are in sound agreement with the steady-state fluorescence experiments (*vide supra*). From these results we hypothesize that an additional deactivation pathway, namely population of a structurally relaxed state with charge transfer implications dominates (*vide infra*) over fluorescence or intersystem crossing in the more polar solvents.

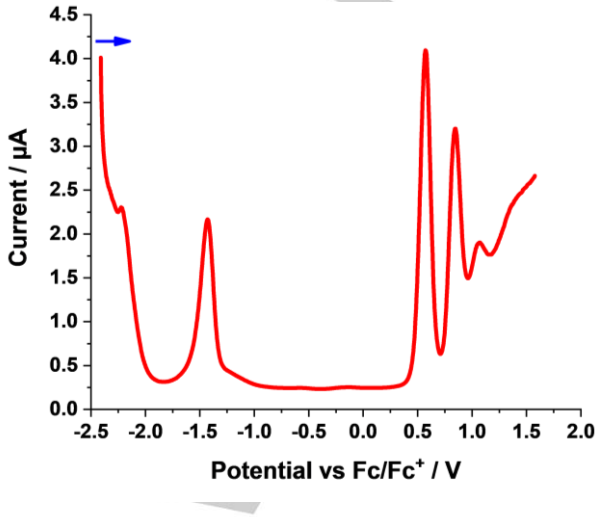

Figure 4. Differential pulse voltammogram of **3** in argon saturated dichloromethane (1.5×10^{-3} M) with 0.1 M $TBAPF_6$ at 0 °C. The blue arrow indicates the scan direction.

Electrochemistry

Electrochemical studies on **3**–**6** were performed in argon saturated dichloromethane (DCM), containing 0.1 M Tetrabutylammoniumhexafluorophosphate ($TBAPF_6$) as supporting electrolyte, at 0 °C. For DPP **3**, we observe two oxidations at +0.57 and +0.85 V vs Fc/Fc^+ and two reductions at −1.43 and −2.22 V vs Fc/Fc^+ (Figure 4; Table 4). The same holds for **4** with the oxidations being at +0.84 and +1.09 V vs Fc/Fc^+ and the reductions being at −1.17 and −1.45 V vs Fc/Fc^+ (Figure S9; Table 4). However, for **5** and **6** three reductions rather than two are observable next to the two oxidations (Figures S10 and S11; Table 4). We hypothesize that the additional reduction for **5** and **6**, which are the fully conjugated DPPs, are attributed to their extended π-systems when compared to **3** and **4**. The electrochemical gaps range from 1.83 eV for **6** to 2.01 eV for **4** (Table 4) and match quite well with the optical gaps derived from steady state absorption experiments.

Table 3. TCSPC lifetimes, at each respective excitation and emission wavelength in toluene and benzonitrile.

	Toluene			Benzonitrile	
3	λ_{Exc} = 520 nm	1.8 ns	λ_{Em} = 575 nm	<0.2 ns	λ_{Em} = 575 nm
4	λ_{Exc} = 530 nm	4.2 ns	λ_{Em} = 590 nm	<0.2 ns	λ_{Em} = 590 nm
5	λ_{Exc} = 555 nm	4.1 ns	λ_{Em} = 620 nm	<0.2 ns	λ_{Em} = 620 nm
6	λ_{Exc} = 595 nm	3.7 ns	λ_{Em} = 670 nm	<0.2 ns	λ_{Em} = 670 nm

Table 4. Oxidations, reductions, and electrochemical gaps in dichloromethane, derived from DPV. All values are given vs Fc/Fc^+.

	Ox_2 / V	Ox_1 / V	Red_1 / V	Red_2 / V	Red_3 / V	E_{gap} / eV
3	0.85	0.57	−1.43	−2.22	-	2.00
4	1.09	0.84	−1.17	−1.45	-	2.01

5	0.78	0.53	−1.36	−1.56	−2.02	1.89
6	0.83	0.58	−1.25	−1.60	−2.05	1.83

Spectroelectrochemistry

To get insights into the spectroscopic features of the oxidized and reduced species of **3**-**6**, spectroelectrochemistry was performed in argon saturated benzonitrile, containing 0.1 M $TBAPF_6$ as supporting electrolyte (see Supplementary Figure S12-15). Figure S12 shows the differential absorption spectra of **3** in benzonitrile upon applying a potential of +1.2 V (Figure S12, top) and −1.0 V (Figure S12, bottom) to generate the one-electron oxidized and reduced form of **3**, respectively. The black spectra in Figures S12-15 represent the reference spectra prior to any potential and, therefore, serve as baselines. Upon oxidation of **3** (Figure S12, top), ground state bleaching (GSB) at 528 and 573 nm, which mirror the absorption spectrum, is discernable. In addition, three characteristic maxima arise at 329, 607, and 737 nm. Major changes in the absorption spectrum are also observed upon reduction of **3** (Figure S12, bottom). GSB is observed at 527 and 571 nm. Furthermore, two maxima develop at 415 and 631 nm. It should be noted that the optical absorption spectra of the oxidized and reduced species of **3**-**6** look quite similar and are comparable to other spectroelectrochemically investigated DPPs.[10f]

First principle calculations

We have performed *ab initio* studies using a protocol combining Time-Dependent Density Functional Theory (TD-DFT) and second-order Coupled-Cluster (CC2) calculations including solvent effects (see the SI). According to DFT, the benzofuran moieties in all compounds are nearly coplanar with the DPP core in both the (S_0) and (S_1) states. Consistently, the electron density difference plots (Figure 5; Supplementary Figure S32) show that the bright lowest excited state corresponds to a π-π* excitation delocalized primarily over the four five-membered rings with no direct contribution from the NO_2 groups. In **3** and **4**, the nitropyridine moiety on the N-atom is strongly twisted compared to the core in both states (e.g., 72.5° and 72.3° for S_0 and S_1 in **1**). In contrast, perfect planarity is restored in the two "fused" dyes with true C_s and C_{2h} minima for **5** and **6**, respectively. The excited state (ES) is partially delocalized on the additional six-membered rings, although the nitro groups are again not directly involved. The NO_2 group(s)' lack of involvement in the electronic transitions is consistent with the moderate to strong fluorescence of all four DPPs in toluene. The changes of total dipole moment computed for the $S_0 \rightarrow S_1$ transition are always small (no CT effect), and the oscillator strength associated with this transition is very large. Therefore, the steady-state absorption and emission spectra correspond to this first ES (see also below). In contrast, for all dyes, the (S_2) state has a clear and strong dipolar or quadrupolar CT character – small oscillator strengths and a large change of the dipole moment in the dipolar molecules (Figure 5; Supplementary Figure S32).

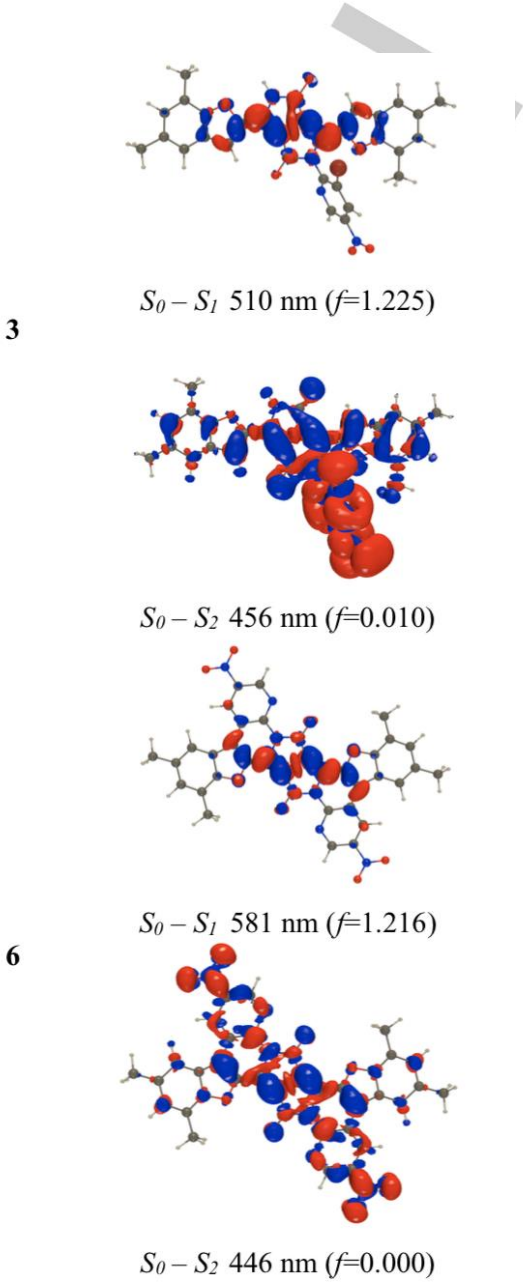

Figure 5. M06-2X density difference plots for the two lowest lying FC ES in dyes **3** and **6**. We recall that the vertical values have no exact experimental counterparts, but the trends in a homologous series are often restored.[29]

In the Franck-Condon (FC) region, this state lies much higher in energy, and is (almost or perfectly) dark, so that it cannot play a role in the steady-state measurements where one notices small Stokes shifts, trifling solvatochromic changes of the transition wavelengths and strong vibronic couplings in all solvents. The computational studies suggest that **3**, after excitation, reaches $(S_1)_{LE}$, but cannot directly deactivate to the CT state. Instead, it

undergoes solvent and structural relaxation before undergoing intersystem crossing (*vide infra*).

In Table 5, we report the vertical and 0-0 energies determined with a composite CC2/TD-DFT approach. We recall that the 0-0 energies can be straightforwardly compared to the experimentally determined crossing point between the absorption and emission.[30,31] The absolute values are within ca. 0.15 eV of the experimental data, typical for such level of theory. More impressive is the agreement in the series. When going from **3** to **4**, only a modest bathochromic displacement of −0.04 eV is computed, in line with −0.03 eV that is seen in the experiments. This shift is due to the inductive effect of the additional pyridine ring(s). Consistently with the experiments, much larger redshifts are obtained for the fused DPPs, with determined displacements of the 0-0 energies −0.15 eV and −0.31 eV for **5** and **6**, as compared to **3**. The experimental values are −0.14 and −0.29 eV.

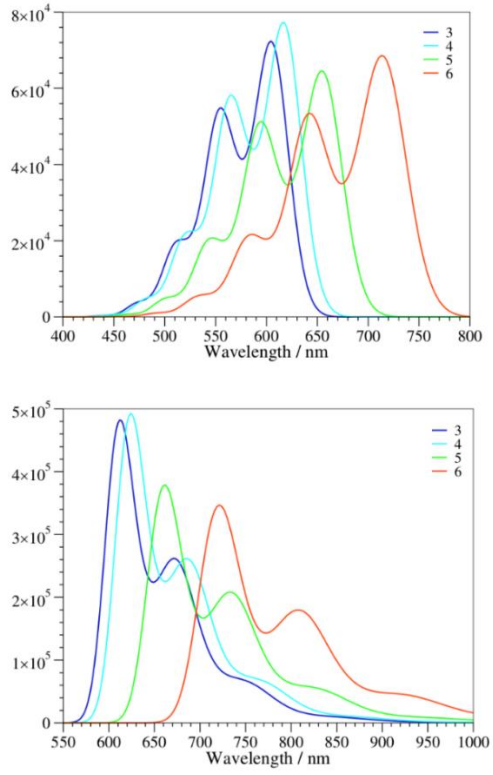

Figure 6. Computed vibrationally resolved spectra for **3**-**6** in toluene: absorption (top) and emission (bottom).

Experimentally, both the absorption and emission spectra show a clear vibronic progression. We accounted for vibronic couplings as described in the SI.[30] As shown in Figure 6, there is an obvious theory-experiment match in terms of band shapes for both absorption and emission, with a clear second maxima and a shoulder at smaller (longer) wavelength for absorption (emission). This confirmed the presence of strong vibronic couplings of similar natures in all compounds. Illustratively, in **6**, the second absorption peak is mainly due to two ES vibrations at 1536 and 1705 cm^{-1}, whereas for emission, only one mode at 1669 cm^{-1} can explain the presence of a second emission peak. All these vibrations correspond to so-called "ECC stretching" modes, in which the nature of single/double bonds in the conjugated core of the dye are modified by the vibrations. The separation between the main and second maxima is therefore ca. 1700 cm^{-1} or 0.21 eV, both experimentally and theoretically.

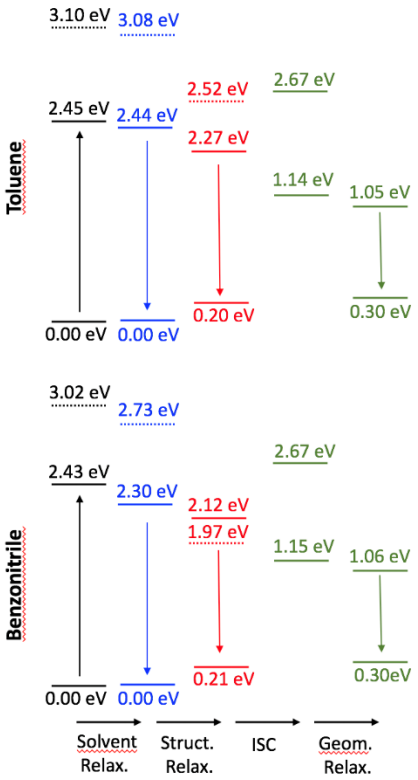

Figure 7. Relative ωB97X-D/6-311+G(2dp) energy levels determined for *N*-arylated DPP **3** in toluene (top) and benzontrile (bottom) with the LR+cLR solvent model, taking the FC point as reference. The full (dashed) lines correspond to the S_1 (S_2) state of dominant local (CT) character. The black values correspond to the FC point, blue data to the relaxed solvent, red to relaxed solvent and structural parameters, whereas the green values are for the triplet ES.

To further investigate the various ES processes, we have performed additional calculations of the relaxation effects (see the SI for details). As the (S_2) state presents a very strong CT character (*vide supra*), we have been careful to use a range-separated hybrid and to account for state-specific solvation effects. An illustration of the behavior obtained is given in Figures 7-8 for DPPs **3** and **6** (see Supplementary Figures S34-S37 for all compounds). First, as expected, the $(S_2)_{CT}$ state undergoes a symmetry breaking process (the symmetric compound becomes unstable in the $(S_2)_{CT}$ after relaxation), and it can be seen that its energy becomes closer to the one of the $(S_1)_{LE}$ state relaxed in the same way, especially for **3** and **4** in benzonitrile for which this CT state becomes even lower in energy. Nevertheless, we underline that experimentally, the used irradiation wavelength in

the experimental set-up (see below) corresponds to the excitation of the dipole-allowed (S_1) so that a fully relaxed (S_2) (as shown in Figure 7) cannot be reached directly. Secondly, the solvent relaxation has a trifling effect in toluene (ca. −0.01 eV), whereas it red-shifts significantly for the lowest excited-state in benzonitrile (ca. −0.15 eV). The subsequent structural relaxation is significant in both solvents, making the structurally relaxed S_1 state 0.34 eV below the original (FC) (S_1) for **6** in benzonitrile, for a much smaller difference of 0.19 eV in toluene for the same dye. From Figure 7 we derive that only the lowest triplet state is accessible for ISC as (T_2) is higher in energy than (S_1). In other words, only one triplet should play a role in the relaxation process. Similar results were obtained for π-expanded DPP **5**.

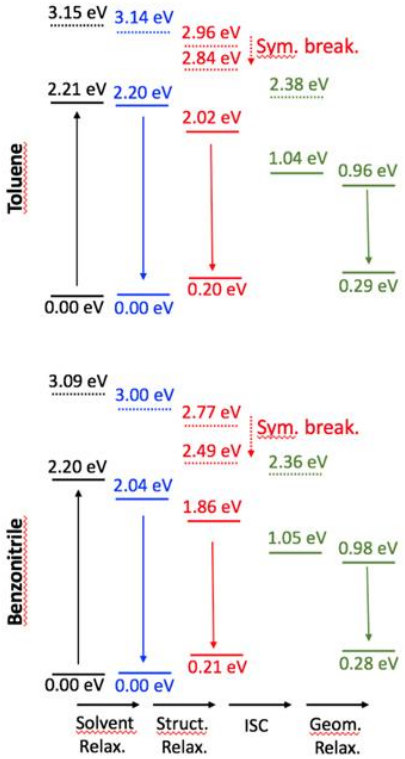

Figure 8. Relative wB97X-D/6-311+G(2dp) energy levels determined for π-expanded DPP **6** in toluene (top) and benzontrile (bottom). See caption of Fig. 7 for more details.

Transient Absorption Spectroscopy

Femtosecond transient absorption (fsTA; 0 – 7500 ps) and nanosecond transient absorption (nsTA; 1 ns – 400 μs, 450 nJ) measurements helped to elucidate the excited state features and kinetics of DPPs **3**-**6**. They were carried out in toluene and benzonitrile with an excitation at 550 nm (fsTA: E = 500 nJ; nsTA: E = 450 nJ). Evaluation of the fsTA and nsTA data was carried out with a combination of multiwavelength and GloTarAn target analyses. Focusing first on the fsTA measurements in toluene, **3**-**6** feature the spontaneous formation of the singlet excited state (S_1). For example, in **3** S_1 includes broad maxima at 450 and 955 nm and minima at 525, 572, and 630 nm corresponding to ground state bleaching (GSB) and stimulated emission (SE), respectively. These features are replaced, on one hand, by a long-lived singlet excited state feature after solvent reorganization has taken place $(S_1)_{SOL}$, and, on the other hand, a short-lived singlet excited state after structural relaxation has taken place $(S_1)_{STR}$. The earlier is caused by the reduction of the solvation energy of the excited state serving as the main driving force, while the latter infers reorganization of the potential energy surface and is likely to possess a sizeable contribution from a redistribution of charge density. The formation of $(S_1)_{STR}$ induces a 8 nm red-shift at the 630 nm GSB and a 28 nm blue-shift and band-narrowing of the maximum at 955 nm. In contrast, $(S_1)_{SOL}$ causes a 4 nm GSB blue-shift and a 28 nm blue-shift and narrowing of the 630 and 970 nm features, respectively.

Table 5. Vertical transition energies (eV) and wavelengths (in nm) determined for the absorption and emission processes in dyes **3**-**6**. On the right-hand-side, we also provide the 0-0 energies obtained theoretically and measured experimentally. All results used a composite CC2/TD-M006-2X approach and are obtained in toluene.

	Absorption		Fluorescence		0-0 energies		
	ΔE / eV	λ / nm	ΔE / eV	λ / nm	ΔE / eV	λ / nm	ΔE / nm / Exper.
3	2.430	510	2.139	580	2.034	610	571
4	2.375	522	2.100	590	1.995	622	580
5	2.294	541	1.999	620	1.881	659	612
6	2.133	581	1.851	670	1.724	719	660

Table 6. fsTa and nsTA lifetimes of dyes **3**-**6** in toluene and benzonitrile.

		$\tau(S_1)$	$\tau(S_1)_{STR}$ / Tol	$\tau(S_1)_{SOL}$	$\tau(S_1)_{STR}$ / BN	$\tau(T_1)$
Toluene	**3**	20.78 ps	244.95 ps	2.35 ns	-	19.19 μs
	4	3.68 ps	119.29 ps	1.49 ns	-	21.14 μs
	5	1.38 ps	269.38 ps	2.86 ns	-	21.89 μs
	6	8.60 ps	228.41 ps	3.93 ns	-	69.94 μs
Benzonitrile	**3**	3.14 ps	-	8.43 ps	19.19 ns	133.86 μs

4	5.19 ps	-	13.46 ps	23.38 ns	13.58 µs
5	8.60 ps	-	24.30 ps	22.03 ns	117.56 µs
6	3.17 ps	-	143.00 ps	13.82 ns	4.16 µs

Similar GSBs and SEs are found for DPPs **4**–**6** in the visible region (Supplementary Figures S16-S22). These shifted in line with the respective steady-state absorption and emission measurements. Strong differences are, however, noted in the NIR region.

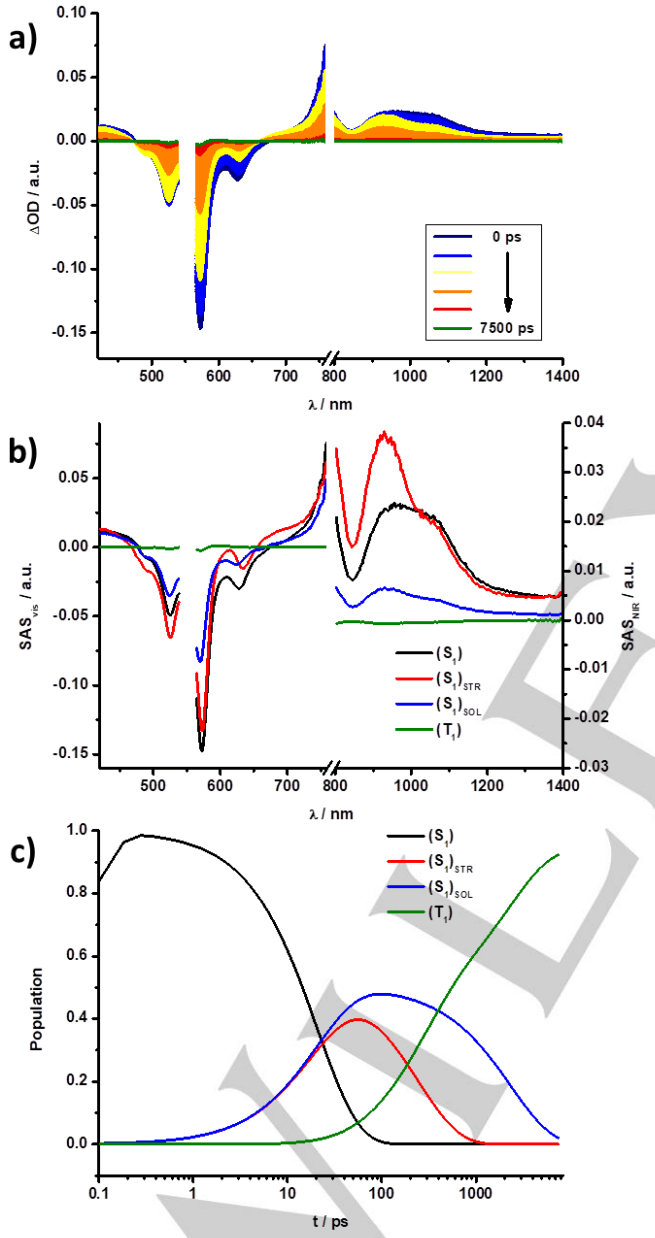

Figure 9. (a) Differential absorption spectra obtained upon fsTA experiments (550 nm) of **3** in toluene with several time delays between 0 and 7500 ps at rt. (b) Species associated spectra of the transient absorption data of **3** shown in a), with the initially formed singlet excited state (S_1) (black), structurally relaxed singlet excited state $(S_1)_{STR}$ (red), solvent reorganized singlet excited state $(S_1)_{SOL}$ (blue), and the triplet excited state (T_1) (green) obtained from GloTarAn. (c) Relative population kinetics of the respective states.

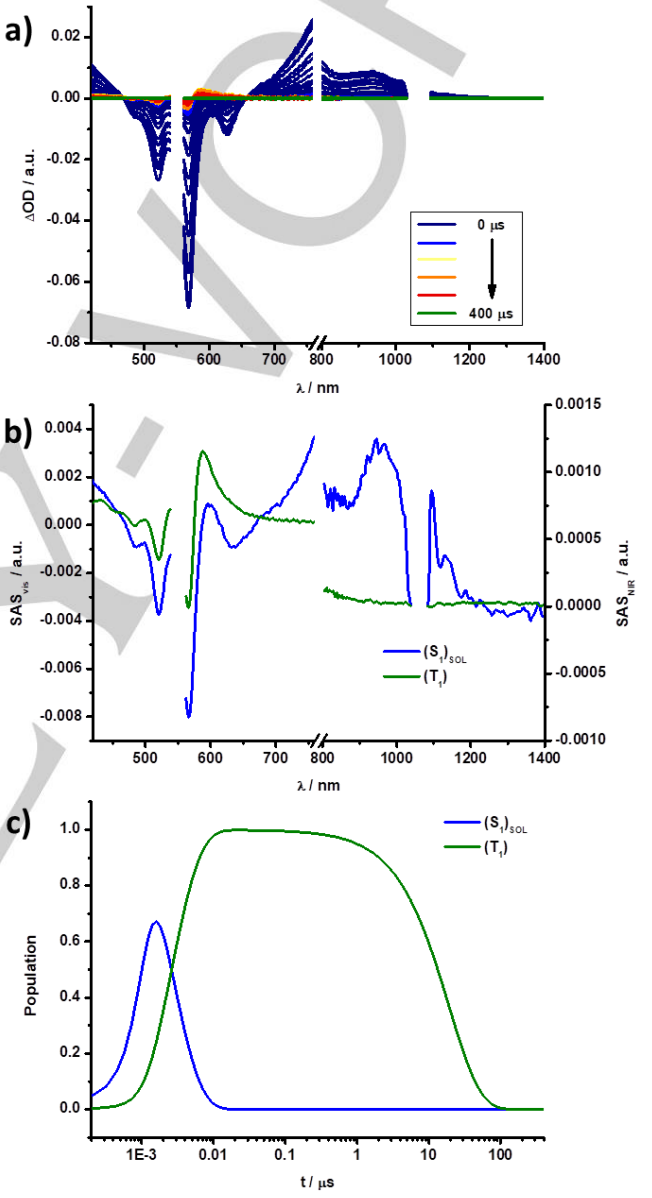

Figure 10. (a) Differential absorption spectra obtained upon nsTA experiments (550 nm) of **3** in toluene with several time delays between 0 and 400 µs at rt. (b) Species associated spectra of the transient absorption data of **3** shown in a), with the solvent reorganized singlet excited state $(S_1)_{SOL}$ (blue), and the triplet excited state (T_1) (green) obtained from GloTarAn. (c) Relative population kinetics of the respective states.

DPP **4** still features a broad maximum at about 1045 nm. Expanded DPPs **5** and **6** feature a narrower fine structure; with

maxima at 894 and 1142 nm for **5**, and 925 and 1152 nm for **6**. We attribute these differences, on the one hand, to the flexible nature of the non-bridged substituents of the DPP-core in **3** and **4**. The immediate consequence is a broader feature in the NIR region. On the other hand, the rigidity in **5** and **6** leads to a narrow $S_0 \rightarrow S_1$ transition and fine structure of the NIR bands. Similar shifts were noted for the remaining transitions. We postulate that for **3**–**6** in toluene, a parallel population of $(S_1)_{SOL}$ and $(S_1)_{STR}$ from (S_1) exists, based on the fact that the energy levels are very close. This was independently confirmed in electrochemical measurements and theoretical calculations. Similar $(S_1)_{SOL}$ and $(S_1)_{STR}$ energies enable significant mixing between them and, in turn, strong and long-lived fluorescent deactivation – vide supra – in toluene.

Both states, in turn, decay into a fourth species, which we assign to a triplet excited state (T_1), via intersystem crossing (ISC). Its growth and decay on the μs timescale is easily followable in the respective nsTA measurements. The spin-forbidden ISC and, in turn, inefficient singlet to triplet excited state transformation results in weak and rather poorly resolved triplet excited state features in **3**–**6**. They consist of GSB and a maximum, which is, for instance in **3**, at 590 nm. In all cases, the same overall shape for (T_1) is a feature. Figures 9 and 10 showcase the fsTA and nsTA spectra of **3** in toluene, respectively.

Changing the solvent to benzonitrile led to significant changes (Supplementary Figures S23-S30). Importantly, the initial S_1 population remains the same, but the subsequent deactivation cascade changes. In particular, $(S_1)_{SOL}$, which is populated initially, transforms into $(S_1)_{STR}$. A significant change in lifetimes is also noted. $(S_1)_{SOL}$ decays in benzonitrile on the picosecond timescale. This is also reflected in the TCSPC measurements, which, in turn, helped in identifying $(S_1)_{SOL}$ in the respective solvent despite the drastically different lifetimes. On the contrary, the $(S_1)_{STR}$ state appeared in benzonitrile, as a result of lowering its energy level, to be stabilized. The parallel deactivation is replaced by a sequential deactivation due to a lower $(S_1)_{STR}$ energy. A potential mixing with $(S_2)_{STR}$ cannot be ruled out. The last steps, namely ISC to (T_1) and recovery of (S_0), remained unchanged. A complete overview of the respective lifetimes in each solvent is given in Table 6.

Conclusions

In this work, we have opened a new avenue towards structurally unique, χ-shaped, π-expanded diketopyrrolopyrroles by means of intramolecular direct arylation as a pivotal step. Our strategy was based on the presence of four functional groups, which had to be present in the structure: two activating electron-withdrawing groups, one fluorine atom, and one bromine atom. More importantly all of them had to be in a suitable arrangement. A two-step process transforms the parent DPP into structures comprising of up to 10 fused rings. As a consequence, the absorptions are bathochromically shifted to the deep-red region and strong red emission is seen despite the presence of NO_2 groups. The latter are inactive in the $S_0 \rightarrow S_1$ electronic transition, even when fused to the DPP core, resulting in strong fluorescence in non-polar solvents with quantum yields to range from 6% to 88% and lifetimes on the order of several nanoseconds. Although in polar solvents the quantum yields are between 0.4% and 3.2% and the lifetimes are on the order of tens of picoseconds the NO_2 groups have literally no impact. As such, the presence of NO_2 groups fails to impose any charge-transfer character on the (S_1) state. This character is only present in the (S_2) state, which was, however, not probed experimentally. Instead, time-resolved techniques and computational studies document that internal conversion and intersystem crossing to afford a structurally relaxed $(S_1)_{STR}$ with a sizeable charge transfer contribution and (T_1), respectively, are responsible for the fluorescence quenching in both *N*-nitroaryl-DPPs and π-expanded DPPs. These results are not only of theoretical significance in that they provide new insights into factors stemming from NO_2 groups and influencing the fluorescent properties, but they may also open the door to design of nitro-aromatics possessing strong and tunable fluorescence. The perspective applications of these novel π-expanded DPPs include, but they are not limited to, low band gap copolymers,[19a] NIR organic field-effect transistors,[18c,19b] solution-processed solar cells[19c] and NIR organic light-emitting diodes for visible light communication.[19e]

Acknowledgements

We thank for financial support from the Foundation for Polish Science (TEAM POIR.04.04.00-00-3CF4/16-00) and from Global Research Laboratory Program (2014K1A1A2064569) through the National Research Foundation (NRF) funded by Ministry of Science, ICT & Future Planning, Korea. K.S. thanks the Foundation for Polish Science for a START scholarship and internship abroad program (START 98.2016). This work used the resources of the CCIPL computational center installed in Nantes.

Keywords: Dyes/Pigments • Lactams • Donor-acceptor systems • Diketopyrrolopyrroles • Fluorescence

1 (a) M. Stępień, E. Gońka, M. Żyła, N. Sprutta, *Chem. Rev.* **2017**, *117*, 3479–3716; (b) Y. S. Park, D. J. Dibble, J. Kim, R. C. Lopez, E. Vargas, A. A. Gorodetsky, *Angew. Chem. Int. Ed.* **2016**, *55*, 3352-3355; (c) F. Chen, Y. S. Hong, S. Shimizu, D. Kim, T. Tanaka, A. Osuka, *Angew. Chem. Int. Ed.* **2015**, *54*, 10639–10642; (d) S. Mishra, M. Krzeszewski, C. A Pignedoli, P. Ruffieux, R. Fasel, D. T. Gryko, *Nat. Commun*. **2018**, *9*, 1714; (e) E. Gońka, P. J. Chmielewski, T. Lis, M. Stępień, *J. Am. Chem. Soc.* **2014**, *136*, 16399–16410; (f) T. Hensel, N. N. Andersen, M. Plesner, M. Pittelkow, *Synlett* **2016**, *27*, 498; (g) K. P. Kawahara, W. Matsuoka, H. Ito, K. Itami, *Angew. Chem. Int. Ed.* **2020**, *59*, 6383-6388; (h) M. K. Węcławski, M. Tasior, T. Hammann, P. J. Cywiński, D. T. Gryko, *Chem. Commun.* **2014**, *50*, 9105–9108; (i) K. Oki, M. Takase, S. Mori, H. Uno, *J. Am. Chem. Soc*. **2019**, *141*, 16255-16259; (j) J. Fan, L. Zhang, A. L. Briseno, F. Wudl, *Org. Lett*. **2012**, *14*, 1024-1026; (k) W. Delaunay, R. Szűcs, S. Pascal, A. Mocanu, P.-A. Bouit, L. Nyulászi, M. Hissler, *Dalton Trans*. **2016**, *45*, 1896; (l) M. Navakouski, H. Zhylitskaya, P. J. Chmielewski, T. Lis, J. Cybińska, M. Stępień, *Angew. Chem. Int. Ed*. **2019**, *58*, 4929-4933.

2 (a) G. E. Rudebusch, A. G. Fix, H. A. Henthorn, C. L. Vonnegut, L. N. Zakharov, M. M. Haley, *Chem. Sci*. **2014**, *5*, 3627; (b) A. Jr. Caruso, J. D. Tovar, *Org. Lett*. **2011**, *13*, 3106; (c) G. Li, Y. Wu, J. Gao, J. Li, Y. Zhao, Q. Zhang, *Chem. Asian J*. **2013**, *8*, 1574; (d) J. Shao, Z. Guan, Y. Yan, C. Jiao, Q.-H. Xu, C. Chi, *J. Org. Chem*. **2011**, *76*, 780; (e) U. Scherf, *J. Mater. Chem*. **1999**, *9*, 1853; (f) A. Fukazawa, S. Yamaguchi, *Chem. Asian J*. **2009**, *4*, 1386.

3 (a) J. Fabian, H. Nakazumi, M. Matsuoka, *Chem. Rev*. **1992**, *92*, 1197-1226; (b) K. J. Fallon, N. Wijeyasinghe, N. Yaacobi-Gross, R. S. Ashraf, D. M. E. Freeman, R. G. Palgrave, M. Al-Hashimi, T. J. Marks, I. McCulloch, T. D. Anthopoulos, H. Bronstein, *Macromolecules* **2015**, *48*, 5148–5154.

4 (a) M. J. Robb, S.-Y. Ku, F. G. Brunetti, C. J. Hawker, *J. Polym. Sci., Part A: Polym. Chem.* **2013**, *51*, 1263-1271; (b) E. D. Głowacki, G. Voss, N. S. Sariciftci, *Adv. Mater.* **2013**, *25*, 6783-6800.

5 R. Stadler, J. Mei, K. R. Graham, L. A. Estrada, J. R. Reynolds, *Chem. Mater.* **2014**, *26*, 664–678.

6 E. D. Głowacki, G. Romanazzi, C. Yumusak, H. Coskun, U. Monkowius, G. Voss, M. Burian, R. T. Lechner, N. Demitri, G. J. Redhammer, N. Sünger, G. P. Suranna, S. Sariciftci, *Adv. Funct. Mater*. **2015**, *25*, 776-787.

7 (a) M. Grzybowski, I. Deperasińska, M. Chotkowski, M. Banasiewicz, A. Makarewicz, B. Kozankiewicz, D. T. Gryko, *Chem. Commun.* **2016**, *52*, 5108-5111; (b) B. Sadowski, H. Kita, M. Grzybowski, K. Kamada, D. T. Gryko, *J. Org. Chem.* **2017**, *82*, 7254−7264.

8 (a) S. Qu, H. Tian, *Chem. Commun.* **2012**, *48*, 3039-3051; (b) M. Grzybowski, D. T. Gryko, *Adv. Opt. Mater*. **2015**, *3*, 280.

9 (a) Z. Ni, H. Wang, H. Dong, Y. Dang, Q. Zhao, X. Zhang, W. Hu, *Nat. Chem*. **2019**, *11*, 271–277; (b) P. Roy, A. Jha, V. B. Yasarapudi, T. Ram, B. Puttaraju, S. Patil, J. Dasgupta, *Nat. Commun*. **2017**, *8*, 1716.

10 (a) M. Grzybowski, E. Glodkowska-Mrowka, V. Hugues, W. Brutkowski, M. Blanchard-Desce, D. T. Gryko, *Chem. Eur. J*. **2015**, *21*, 9101; (b) S. Luňák Jr., J. Vyňuchal, M. Vala, L. Havel, R. Hrdina, *Dyes Pigm*. **2009**, *82*, 102; (c) T. Yamagata, J. Kuwabara, T. Kanbara, *Heterocycles* **2014**, *89*, 1173-1181; (d) A. Purc, B. Koszarna, I. Iachina, D. H. Friese, M. Tasior, K. Sobczyk, T. Pędziński, J. Brewer, D. T. Gryko, *Org. Chem. Front*. **2017**, *4*, 724-736; (e) O. Vakuliuk, A. Purc, G. Clermont, M. Blanchard-Desce, D. T. Gryko, *ChemPhotoChem* **2017**, *1*, 243-252; (f) M. Gora, S. Pluczyk, P. Zassowski, W. Krzywiec, M. Zagorska, J. Mieczkowski, M. Lapkowski, A. Pron, *Synth. Met*. **2016**, *216*, 75–82.

11 (a) Y. Li, P. Sonar, L. Murphy, W. Hong, *Energy Environ. Sci.* **2013**, *6*, 1684; (b) L. Burgi, M. Turbiez, R. Pfeiffer, F. Bienewald, H. J. Kirner, C. Winnewisser, *Adv. Mater*. **2008**, *20*, 2217; (c) M. Tantiwiwat, A. Tamayo, N. Luu, X. D. Dang, T. Q. Nguyen, *J. Phys. Chem. C* **2008**, *112*, 17402; (d) S. L. Suraru, U. Zschieschang, H. Klauk, F. Würthner, *Chem. Commun*. **2011**, *47*, 1767; (e) B. Tieke, A. R. Rabindranath, K. Zhang, Y. Zhu, *Beilstein J. Org. Chem.* **2010**, *6*, 830; (f) M. M. Wienk, M. Turbiez, J. Gilot, R. A. J. Janssen, *Adv. Mater*. **2008**, *20*, 2556; (g) O. Kwon, J. Jo, B. Walker, G. C. Bazan, J. H. Seo, *J. Mater. Chem. A* **2013**, *1*, 7118.

12 (a) A. Purc, E. M. Espinoza, R. Nazir, J. J. Romero, K. Skonieczny, A. Jeżewski, J. M. Larsen, D. T. Gryko, V. I. Vullev, *J. Am. Chem. Soc*. **2016**, *138*, 12826-12832; (b) M. Krzeszewski, E. M. Espinoza, C. Červinka, J. B. Derr, J. A. Clark, D. Borchardt, G. J. O. Beran, D. T. Gryko, V. I. Vullev, *Angew. Chem. Int. Ed*. **2018**, *57*, 12365-12369.

13 (a) A. C. Rochat, L. Cassar, A. Iqbal, *Eur. Pat. Appl.* 94911, **1983**; (b) H. Langhals, T. Grundei, T. Potrawa, K. Polborn, *Liebigs Ann*. **1996**, 679; (c) C. J. H. Morton, R. Gilmour, D. M. Smith, P. Lightfoot, A. M. Z. Slawin, E. J. MacLean, *Tetrahedron* **2002**, *58*, 5547-5565; (d) M. Pieczykolan, B. Sadowski, D. T. Gryko, *Angew. Chem. Int. Ed.* **2020**, *59*, 7528-7535.

14 B. He, A. B. Pun, D. Zherebetskyy, Y. Liu, F. Liu, L. M. Klivansky, A. M. McGough, B. A. Zhang, K. Lo, T. P. Russell, L. Wang, Y. Liu, *J. Am. Chem. Soc.* **2014**, *136*, 15093–15101.

15 G. M. Fischer, A. P. Ehlers, A. Zumbusch, E. Daltrozzo, *Angew. Chem. Int. Ed.* **2007**, *46*, 3750.

16 (a) S. Shimizu, T. Iino, Y. Araki, N. Kobayashi, *Chem. Commun*. **2013**, *49*, 1621; (b) S. Shimizu, T. Iino, A. Saeki, S. Seki, N. Kobayashi, *Chem. Eur. J.* **2015**, *21*, 2893-2904; (c) S. Shimizu, *Chem. Commun.* **2019**, *55*, 8722-8743; (d) Y. Kage, S. Mori, M. Ide, A. Saeki, H. Furuta, S. Shimizu, *Mater. Chem. Front.* **2018**, *2*, 112.

17 W. Yue, S.-L. Suraru, D. Bialas, M. Müller, F. Würthner, *Angew. Chem. Int. Ed*. **2014**, *53*, 6159–6162.

18 (a) M. Grzybowski, E. Glodkowska-Mrowka, T. Stoklosa, D. T. Gryko, *Org. Lett.* **2012**, *14*, 2670-2673; (b) M. Grzybowski, D. T. Gryko, US20140357869A1, **2015**; (c) D. T. Gryko, M. Grzybowski, P. Hayoz, A. Jeżewski, US9698348B2, **2017**; (d) M. Grzybowski, V. Hugues, M. Blanchard-Desce, D. T. Gryko, *Chem. Eur. J.* **2014**, *20*, 12493-12501.

19 (a) F. Trilling, O. Sachnik, U. Scherf, *Polym. Chem*. **2019,** *10*, 627-632; (b) L. Ma, B. Chen, Y. Guo, Y. Liang, D. Zeng, X. Zhan, Y. Liu, X. Chen, *J. Mater. Chem. C* **2018**, *6*, 13049-13058; (c) B. Chen, Y. Yang, P. Cheng, X. Chen, X. Zhan, J. Qin, *J. Mater. Chem. A* **2015,** *3*, 6894-6900; (d) E. Gońka, L. Yang, R. Steinbock, F. Pesciaioli, R. Kuniyil, L. Ackermann, *Chem. Eur. J*. **2019**, *25*, 16246-16250; (e) A. Minotto, P. A. Haigh, Ł. G. Łukasiewicz, E. Lunedei, D. T. Gryko, I. Darwazeh, F. Cacialli, *Light-Sci. Appl.* **2020**, *9*, 70.

20 (a) T. Ueno, Y. Urano, H. Kojima, T. Nagano, *J. Am. Chem. Soc*. **2006**, *128*, 10640-10641; (b) Y. Ueda, Y. Tanigawa, C. Kitamura, H. Ikeda, Y. Yoshimoto, M. Tanaka, K. Mizuno, H. Kurata, T. Kawase, *Chem. Asian J.* **2013**, *8*, 392-399.

21 (a) F. Terenziani, A. Painelli, C. Katan, M. Charlot, M. Blanchard-Desce, *J. Am. Chem. Soc.* **2006**, *128*, 15742−15755; (b) B. Dereka, A. Rosspeintner, Z. Li, R. Liska, E. Vauthey, *J. Am. Chem. Soc.* **2016,** *138*, 4643-4649; (c) T. Kim, J. Kim, H. Mori, S. Park, M. Lim, A. Osuka, D. Kim, *Phys. Chem. Chem. Phys.* **2017**, *19*, 13970-13977.

22 F. Pop, J. Humphreys, J. Schwarz, L. Brown, A. van den Berg, D. B. Amabilino, *New J. Chem.* **2019**, *43*, 5783-5790.

23 C. J. H. Morton, R. L. Riggs, D. M. Smith, N. L. Westwood, P. Lightfoot, A. M. Z. Slawin, *Tetrahedron* **2005,** *61*, 727–738.

24 K. Gutkowski, C. Azarias, M. Banasiewicz, B. Kozankiewicz, D. Jacquemin, D. T. Gryko, *Eur. J. Org. Chem*. **2018**, 6643-6648.

25 K. Gutkowski, K. Skonieczny, M. Bugaj, D. Jacquemin, D. T. Gryko, *Chem. Asian J.* **2020**, *15*, 1369-1375.

26 G. C. Finger, L. D. Starr, *J. Am. Chem. Soc*. **1959**, *81*, 2674–2675.

27 W. Hagui, H. Doucet, J.-F. Soule, *Chem* **2019**, *5*, 2006–2078.

28 Ł. Łukasiewicz, H. G Ryu, A. Mikhaylov, C. Azarias, M. Banasiewicz, B. Kozankiewicz, K. H Ahn, D. Jacquemin, A. Rebane, D. T. Gryko, *Chem. Asian J*. **2017**, *12*, 1736-1748.

29 A. D. Laurent, C. Adamo, D. Jacquemin, *Phys. Chem. Chem. Phys.* ***2014****, 16*, 14334–14356.

30 F. Santoro, D. Jacquemin, *Wires Comput. Mol. Sci.* **2016**, *6*, 460–486.

Entry for the Table of Contents

RESEARCH ARTICLE

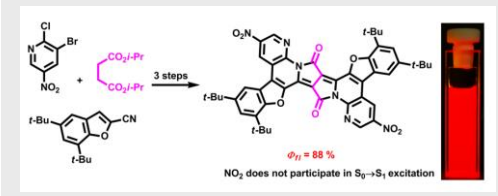

The fluorescence of centrosymmetric, π-expanded diketopyrrolopyrroles possessing 10 conjugated rings is not quenched in non-polar solvents as a result of the lack of participation of NO_2 groups in electronic transitions and lack of reachable charge-transfer state. A strategy has now been developed to diminish radiationless pathways, so that nitro-aromatics can emit intense red light in solvents of moderate polarity.

Kamil Skonieczny, Ilias Papadopoulos, Dominik Thiel, Krzysztof Gutkowski, Philipp Haines, Patrick M. McCosker, Adèle D. Laurent, Paul A. Keller, Timothy Clark, Denis Jacquemin, Dirk M. Guldi* and Daniel T. Gryko**

Page No. – Page No.

How to Make Nitroaromatics Glow: Next Generation Large, χ—Shaped, Centrosymmetric Diketopyrrolopyrroles